Tension-Aware Error Modeling for Fast Pose Estimation of Underactuated Cable-Driven Parallel Robots

Sara Gabaldo, Edoardo Idà, and Marco Carricato

Abstract Suspended underactuated cable-driven parallel robots may achieve large workspaces, but exhibit limited controllability. Real-time solution of their direct kinematics is essential for model-based control but is challenged by nonlinear constraints, multiple solutions, and high sensitivenes to measurement errors. This paper proposes a sensor-fusion pose-estimation method that exploits redundant measurements within a simple geometric model, while explicitly accounting for the effect of cable tension on measurement uncertainty. A data-driven procedure identifies physically meaningful tension–error relationships, which are used to weight residuals and define termination criteria in a weighted least-squares solver. Experiments on a 4-cable prototype show that a good pose accuracy is achieved with limited computation time.

1 Introduction

Cable-Driven Parallel Robots (*CDPRs*) control an end-effector (*EE*) using actuated cables instead of rigid links [1]. Underactuated *CDPRs* (*UACDPRs*) use fewer cables than the *EE* degrees of freedom (*DoFs*), improving accessibility in suspended layouts at the expense of constraint deficiencies: even

S. Gabaldo
Dept. of Industrial Engineering, University of Bologna, 40137 Bologna, Italy
e-mail: sara.gabaldo3@unibo.it

E. Idà
Dept. of Industrial Engineering, University of Bologna, 40137 Bologna, Italy
e-mail: edoardo.ida2@unibo.it

M. Carricato
Dept. of Industrial Engineering, University of Bologna, 40137 Bologna, Italy
e-mail: marco.carricato@unibo.it

with locked actuators, the *EE* may retain uncontrolled motions and behave as a multi-*DoF* pendulum [2].

The direct kinematics (*DK*) *UACDPRs* the problem is intrinsically underdetermined, making additional sensing necessary. Common measurements include cable tensions, swiveling-pulley angles, and *EE* orientation; tensions are often necessary for control, pulley angles are inexpensive and easily integrated in winches, and orientation sensing is typically required in suspended systems due to the low sensitivity of *EE* orientation to cable-length changes [3]. Combining these signals into a robust pose estimate requires sensor-fusion techniques [4]. Most approaches fuse dynamics and sensor models, though when sensing redundancy and sampling rates are high, geometric and sensor models alone can be equally effective [5].

Alternatively, detailed geometric and dynamic models that account for cable sagging [6] or pulley behavior [7] can reduce sensing requirements, but they demand accurate parameter identification, rely on motion assumptions (e.g., quasi-static), and increase computational cost. This work instead adopts a simplified geometric model with massless, inextensible, straight cables, relying on additional sensing and sensor fusion to compensate for modeling simplifications. Measurement reliability, though, depends on operating conditions: at low tensions, sagging and backlash degrade cable-length and swivel-angle measurements. Here, inspired by [8] where configuration-dependent reliability is incorporated through adaptive residual weighting, we model these errors as functions of cable tension, a key configuration-dependent variable [9].

Building on the sensor-fusion *DK* formulation in [10], this paper proposes a data-driven procedure to learn tension-dependent error models for cable-length and swivel-angle measurements and integrate them into a real-time pose-estimation algorithm. These models define the weighting matrix and componentwise termination thresholds of a weighted least-squares solver, improving convergence speed while preserving accuracy [10].

In the following, Secc 2 introduces the simplified *UACDPR* model. Section 3 presents the sensor-fusion pose-estimation algorithm, Sec. 4 describes the tension-dependent error models. Experimental validation is reported in Sec. 5, followed by conclusions in Sec. 6.

2 *UACDPR* Geometric Model

A generic *UACDPR* consists of a 6-*DoF* *EE* actuated by $n < 6$ cables. $Oxyz$ is an inertial frame and $Px'y'z'$ is attached to the *EE* (Fig. 1a). The *EE* pose is $\boldsymbol{\zeta} = [\mathbf{p}^T \ \boldsymbol{\epsilon}^T]^T$, where $\mathbf{p}$ is the position of the *EE* reference point in $Oxyz$ and $\mathbf{R}(\boldsymbol{\epsilon})$ is the orientation matrix parameterized by rollpitchyaw angles $\boldsymbol{\epsilon} = [\phi, \theta, \psi]^T$. Each cable is wound on a servo-driven winch and modeled as massless and inextensible line, so its length varies proportionally with actu-

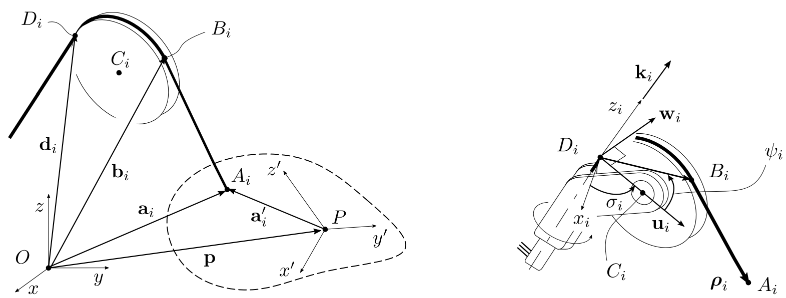

(a) (b)

Fig. 1: *UACDPR* (a) and swivel pulley (b) geometric models

ator displacement [1]. At low tension, cables may deviate from the straight-line assumption due to sagging or local slackness, and backlash can affect sensed quantities; these effects motivate the tension-aware error modeling in Section 4. When cables are lightweight and sufficiently tensioned, however, a straight-segment approximation is reasonable.

Cables are routed from the winches through swivel pulleys. Each pulley rotates about a swivel axis z_i tangent to its groove, has center C_i and radius r_i. The cable enters the groove at a fixed point D_i and exits tangentially at B_i, whose position depends on the *EE* pose, pulley geometry, and cable model. Their position vectors in $Oxyz$ are $\mathbf{d}_i$ and $\mathbf{b}_i$, respectively. The cable attaches to the *EE* at A_i, with inertial position $\mathbf{a}_i = \mathbf{p} + \mathbf{R},^P \mathbf{a}'_i$. Assuming A_i, D_i, and z_i are coplanar, the pulley plane is defined by $\boldsymbol{\varrho}_i = \mathbf{a}_i - \mathbf{d}_i$ and z_i. Thus, the swivel-angle σ_i is

$$\sigma_i = \operatorname{atan2}(\varrho_{i,x},\ \varrho_{i,y}). \tag{1}$$

The tangency angle ψ_i, describing the cable wrap around the pulley, is obtained from the pulley geometry and $\boldsymbol{\varrho}_i$ [10]. The straight cable segment is defined as $\boldsymbol{\rho}_i = \mathbf{b}_i - \mathbf{a}_i$, and the total cable-length is

$$l_i = r_i(\pi - \psi_i) + \|\boldsymbol{\rho}_i\|, \tag{2}$$

where the first term accounts for the arc length wrapped around the pulley. This geometric model is valid only when cables are sufficiently tensioned.

3 *UACDPR* Pose Estimation

Building upon [10], this section presents a pose-estimation framework for solving the direct kinematics (*DK*) of *UACDPRs*, formulated as a weighted nonlinear least-squares problem solved via a Gauss–Newton scheme. At each time instant, a subset of pose-dependent geometric quantities is assumed to be measurable. Let $\mathbf{h}(\boldsymbol{\zeta}) \in \mathbb{R}^m$ collect the modeled quantities and $\mathbf{z} \in \mathbb{R}^m$ the corresponding measurements. In this paper $\mathbf{h}$ comprises cable lengths, swivel angles, and *EE* roll, pitch and yaw angles, and all of them are assumed to be measurable. Therefore:

$$\mathbf{h}(\boldsymbol{\zeta}) = [l_1(\boldsymbol{\zeta}) \dots l_n(\boldsymbol{\zeta}) \;\; \sigma_1(\boldsymbol{\zeta}) \dots \sigma_n(\boldsymbol{\zeta}) \;\; \phi(\boldsymbol{\zeta}) \;\; \theta(\boldsymbol{\zeta}) \;\; \psi(\boldsymbol{\zeta})]^T \tag{3}$$

$$\mathbf{z} = [l_1 \dots l_n \;\; \sigma_1 \dots \sigma_n \;\; \phi \;\; \theta \;\; \psi]^T \tag{4}$$

$$\mathbf{r}(\boldsymbol{\zeta}) = \mathbf{h}(\boldsymbol{\zeta}) - \mathbf{z} \tag{5}$$

The *DK* problem consists in finding the pose vector $\boldsymbol{\zeta}$ that makes $\mathbf{r}(\boldsymbol{\zeta})$ equal to zero. Although a minimum of $m \geq 6$ residual equations is required to match the number of unknowns, this condition alone does not guarantee a reliable solution, as the Jacobian may become rank-deficient or measurement errors may dominate some residuals. For this reason, the sensor-fusion *DK* problem is formulated by considering an overdetermined residual vector $\mathbf{r}(\boldsymbol{\zeta}) \in \mathbb{R}^m$, with $m > 6$, recasted as a weighted nonlinear least-squares optimization:

$$\min_{\boldsymbol{\zeta}} \quad f(\boldsymbol{\zeta}) \qquad \text{with} \quad f(\boldsymbol{\zeta}) = \frac{1}{2}\mathbf{r}^T(\boldsymbol{\zeta})\mathbf{Q}^{-1}\mathbf{r}(\boldsymbol{\zeta}) \tag{6}$$

where $\mathbf{Q} = \mathrm{diag}(q_1 \dots q_m)$ is a diagonal weighting matrix which normalizes the residuals and prevents unit inconsistencies in the dimensionless cost function f.

Let $\mathbf{e} \in \mathbb{R}^m$ collect the scalar uncertainties associated with the measurements in $\mathbf{z}$, where each e_i estimates the expected error of the i-th residual. Depending on the adopted model, e_i may be a constant standard deviation (StD) or a configuration-dependent function (Section 4). The i-th weighting coefficient is defined as $q_i = e_i^{-2}$, so that residuals predicted to be less reliable (large e_i) have lower influence on the descent direction. Given an initial *EE* pose estimate $\boldsymbol{\zeta}_0$, the GaussNewton algorithm updates the solution at iteration k as [10].

$$\boldsymbol{\zeta}_{k+1} = \boldsymbol{\zeta}_k - \left(\mathbf{J}_k^T\mathbf{Q}_k^{-1}\mathbf{J}_k\right)^{-1}\mathbf{J}_k^T\mathbf{Q}_k^{-1}\mathbf{r}_k, \tag{7}$$

where $\mathbf{J}_k = \nabla\mathbf{h}(\boldsymbol{\zeta}_k)$ and $\mathbf{r}_k = \mathbf{r}(\boldsymbol{\zeta}_k)$. The algorithm terminates as soon as one of the following stopping criteria is met:

1. the iteration counter reaches the upper threshold $T_k = 100$;

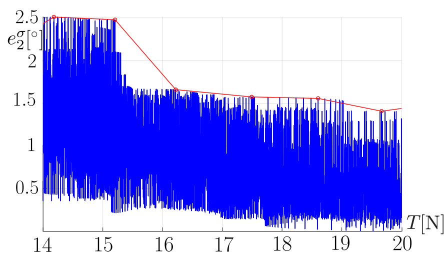

(a)

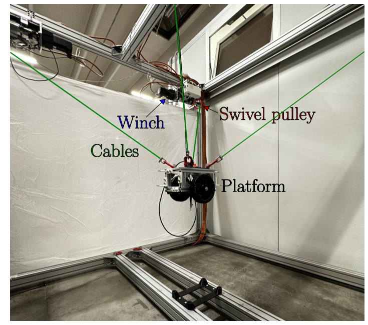

(b)

Fig. 2: Example of wwivel-angle measurement errors (blue) and their peaks (red) versus cable tension (a) and 4-cable suspended *UACDPR* prototype (b, cables are green).

2. the step size becomes negligible, namely $\|\Delta \mathbf{p}_k\| \leq 10^{-6}$ m and $\|\Delta \boldsymbol{\epsilon}_k\| \leq 10^{-6}$ rad;
3. the gradient norm becomes negligible, namely

$$\left\| \left. \frac{\partial f(\boldsymbol{\zeta})}{\partial \mathbf{p}} \right|_{\boldsymbol{\zeta}_k} \right\| \leq 10^{-6}\,\mathrm{m}^{-1} \quad \text{and} \quad \left\| \left. \frac{\partial f(\boldsymbol{\zeta})}{\partial \boldsymbol{\epsilon}} \right|_{\boldsymbol{\zeta}_k} \right\| \leq 10^{-6}\,\mathrm{rad}^{-1}; \qquad (8)$$

4. each residual component $|r_{k,i}|$ falls below its tolerance $T_{\mathbf{r},i}$, $\forall i = 1, \ldots, m$. Each threshold $T_{\mathbf{r},i}$ can be set consistently with the assumed error model, e.g., $T_{\mathbf{r},i} = e_i$, so that reliable measurements enforce stricter convergence while unreliable ones do not hinder termination.

4 Tension-Dependent Error Modeling

This section describes how uncertainty in cable-length and swivel-angle measurements can be modeled using auxiliary signals that indicate measurement reliability, namely cable tension. At low tension, sagging and friction/backlash effects reduce measurement accuracy; therefore, the modeled error is assumed to increase as tension decreases. Two physically meaningful correlation models are proposed for each cable and measurement type: a *linear-in-tension model*

$$e(\tau) = a + b\tau, \qquad b < 0, \qquad (9)$$

where $b < 0$ indicates a decreasing error with tension, and an *inverse-tension model*

$$e(\tau) = \frac{c}{\tau} + d, \tag{10}$$

which penalizes very low tensions and diverges as $\tau \to 0^+$. In the pose-estimation algorithm (Section 3), this divergence effectively discards near-zero-tension measurements by assigning them negligible weight.

To identify the coefficients a, b, c, and d, configurations are sampled throughout the workspace while collecting cable tension τ_i, cable length l_i, and swivel angle σ_i. A ground-truth *EE* pose $\boldsymbol{\zeta}gt$ is required to compute reference values $l_i(\boldsymbol{\zeta}gt)$ and $\sigma_i(\boldsymbol{\zeta}gt)$ via the inverse geometric model (Section 2). Measurement-error samples are then computed as

$$e_i^l = |l_i - l_i(\boldsymbol{\zeta}gt)|, \qquad e_i^\sigma = \left|\sigma_i - \sigma_i(\boldsymbol{\zeta}_{gt})\right|. \tag{11}$$

For each cable, triplets $(\tau_i, e_i^l, e_i^\sigma)$ are sorted by increasing τ_i. To obtain a conservative tensionerror relation, samples are grouped into fixed-width tension intervals and only the maximum error in each interval is retained. This preserves the worst-case measurement error rather than the average behavior.

Figure 2a illustrates the process for the swivel-angle error of one cable. The blue curve shows all measured errors versus tension, while red markers denote the peak error in each 1 N interval used for regression. The coefficients a, b, c, and d are then identified through a density-aware weighted least-squares fit (KDE-based weights [12]).

5 Experimental Validation on a 4-Cable *UACDPR* Prototype

The proposed tension-aware pose-estimation algorithm is experimentally validated on a 4-cable, 6-*DoF UACDPR* prototype at the University of Bologna (Fig. 2b). This architecture is particularly challenging because stability and controllability depend critically on maintaining cable tension. The experimental setup, sensing architecture, and dataset are the same as in [10], enabling direct comparison with the constant-StD baseline reported there.

Measurements were collected over $73,891$ quasi-static configurations while the *EE* followed a workspace-scanning trajectory composed of linear segments at 1 cm/s. The dataset covers a wide tension range, from taut to near-slack cables, and includes synchronized measurements of cable lengths, swivel angles, *EE* orientation, and cable tensions. Cable lengths are estimated from motor encoders through the motor kinematic model (resolution $\sim$ 0.1 cm) [13]. Swivel angles are measured by encoders on the swivel axes (resolution $\sim 0.02°$). An AHRS inclinometer (XSens MTi-630) mounted on the *EE* provides roll ϕ and pitch θ (accuracy $\sim 0.5°$) and yaw ψ (accuracy $\sim 3°$). Cable tensions are measured using load cells (accuracy $\sim$ 5 N). The ground-

Table 1: Measurement error models for the 4-cable prototype

Cable-lenght error models:

Cable	Standard deviation [cm]	Linear error model [cm]	Inverse error model [cm]
1	0.39	$0.9213 - 0.0038\,\tau_1$	$0.30 + 20.68/\tau_1$
2	0.26	$0.7164 - 0.0054\,\tau_2$	$0.04 + 17.11/\tau_2$
3	0.10	$0.2090 - 0.0002\,\tau_3$	$0.16 + 2.22/\tau_3$
4	0.15	$0.3877 - 0.0014\,\tau_4$	$0.24 + 2.68/\tau_4$

Swivel-angle error models:

Cable	Standard deviation [°]	Linear error model [°]	Inverse error model [°]
1	0.22	$0.6066 - 0.0024\,\tau_1$	$0.2717 + 9.2740/\tau_1$
2	0.62	$1.6844 - 0.0106\,\tau_2$	$0.6011 + 19.5473/\tau_2$
3	0.28	$0.7017 - 0.0026\,\tau_3$	$0.3102 + 10.7300/\tau_3$
4	0.38	$0.8340 - 0.0050\,\tau_4$	$0.3229 + 8.6496/\tau_4$

truth *EE* pose $\boldsymbol{\zeta}gt = [\mathbf{p}gt^T; \boldsymbol{\epsilon}gt^T]^T$ is reconstructed from nine *EE*-mounted reflective markers tracked by a Vicon system (marker accuracy ± 0.2 mm). Using the geometric model in Section 2, reference cable lengths $l_i(\boldsymbol{\zeta}gt)$ and swivel angles $\sigma_i(\boldsymbol{\zeta}_{gt})$, $i = 1 \ldots 4$, are computed from the ground-truth pose, allowing measurement errors to be evaluated as in Eq. (11).

Three error models are considered (Sections 34): (i) a baseline model where errors are Gaussian with *constant StD*, computed as in [10], (ii) a *linear-in-tension model* (Eq. (9)), (iii) an *inverse-tension model* (Eq. (10)). Table 1 reports the identified parameters for the prototype. Cable-length regressions are shown in Fig. 3a, and swivel-angle regressions in Fig. 3b. In some cases the linear model better captures the trend (e.g., e^l_2, e^l_3, e^σ_3), while in others the inverse model fits more accurately (e.g., e^σ_2), indicating that the most suitable correlation depends on the specific cable and sensor. Figure 3 shows representative tensionerror relationships from the dataset. Orientation measurements from the AHRS exhibit approximately Gaussian, tension-independent errors and are therefore modeled with constant StDs: $e_\phi = 0.30°$, $e_\theta = 0.16°$, $e_\psi = 0.35°$ [10].

In the following, the impact of the three measurement-error modeling strategies on the performance of the pose-estimation algorithm introduced in Section 3 is evaluated. Table 2 reports the pose-estimation accuracy obtained with the three considered error models, evaluated on the same experimental dataset used to test the pose estimation algorithm. Results show that all models achieve comparable accuracy, with average position errors below 0.7 cm and average orientation errors below 0.5°. A comparable behavior is observed for the maximum errors, which remain within a limited range across all error models. Notably, the inverse-tension error model yields larger maximum errors, which is consistent with its more aggressive down-weighting of low-tension measurements, occasionally reducing the informative residual set. On the other hand, the average computation time decreases from 8.4 ms with a

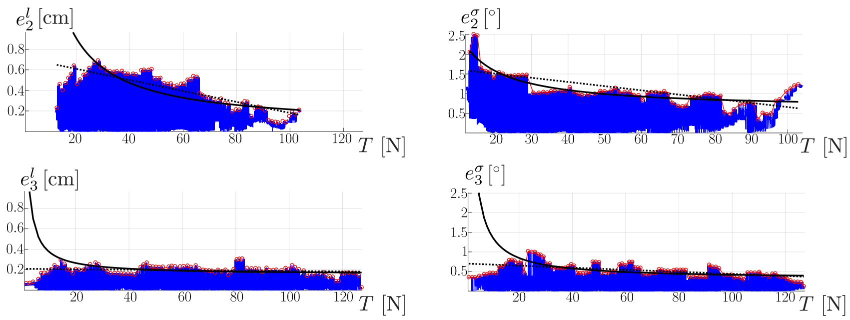

(a) (b)

Fig. 3: Representative linear (a) and inverse (b) tensionerror correlations: measured errors (blue), selected peak values (red), and fitted regressions (black), illustrating accurate fits and model limits.

Table 2: Impact of the measurement-error modeling strategies on pose-estimation performance

Pose estimation accuracy:

	Standard deviation	Linear error model	Inverse error model
Avg. position error [cm]	0.571	0.616	0.658
Max. position error [cm]	1.260	1.438	1.679
Avg. orientation error [°]	0.431	0.465	0.496
Max. orientation error [°]	0.849	0.907	0.980

Computation time and iteration count:

	Standard deviation	Linear error model	Inverse error model
Avg. time [ms]	8.4	3.6	3.7
Max. time [ms]	39.8	37.3	28.3
Avg. iter. [–]	3.047	0.824	0.689
Max. iter. [–]	5	5	5

constant StD to about 3.6–3.7 ms with tension-aware models, achieving more than 55% reduction, while the average Gauss-Newton

iteration count drops from ~ 3.0 to below 1. These results indicate that tension-aware error modeling primarily improves convergence properties and computational efficiency rather than pose-estimation accuracy: reliable (high-tension) residuals dominate the descent direction and termination conditions, while low-tension measurements are progressively down-weighted.

6 Conclusions

This paper presented a tension-aware, geometry-based pose-estimation method for underactuated *CDPRs*. Instead of increasing model complexity (e.g., modeling cable sagging), the approach exploits redundant measurements, cable lengths, swiveling-pulley angles, and *EE* orientation, and models their reliability as a function of cable tensions within a weighted nonlinear least-squares solver. A data-driven procedure identifies tension-dependent error models for cable-length and swivel-angle measurements, used both for residual weighting and componentwise termination thresholds. Experiments on a 4-cable prototype show that this strategy preserves pose-estimation accuracy while significantly improving convergence speed. Compared with a baseline, the average computation time per *DK* solution is reduced by over 50%, and the average number of GaussNewton iterations drops to about one third, confirming suitability for real-time implementation.

Future work will expand the experimental dataset, targeting extreme operating conditions such as near-slack cables and workspace boundaries, and investigate alternative error-correlation models (e.g., higher-order polynomials or neural networks). The tension-aware framework will also be validated on other cable-driven architectures, including overactuated systems, to assess generality and scalability.

References

1. Idà, E., Mattioni, V.: Cable-driven parallel robot actuators: State of the art and novel servo-winch concept. Actuators 11(10) (2022) DOI: 10.3390/act11100290
2. Angelini, M., Idà, E., Bertin, D., Mantovani, E., Bazzi, D., Orassi, V., Carricato, M: An underactuated cable-driven parallel robot for marine automated launch and recovery operations. ASME Journal of Mechanisms and Robotics, 17(1), Paper No. 010906, pp. 1-10 (2025) DOI: 10.1115/1.4065394
3. Gabaldo, S., Idà, E., Carricato, M.: Sensitivity of the direct kinematics of underactuated cable-driven parallel robots to redundant sensor-measurement errors. In: Altuzarra, O., Kecskeméthy, A. (eds.) Advances in Robot Kinematics 2022. Springer Proceedings in Advanced Robotics, vol 24, pp. 131138. Springer (2022) DOI: 10.1007/978-3-031-08140-8_15
4. Garant, X., Campeau-Lecours, A., Cardou, P., Gosselin, C.: Improving the forward kinematics of cable-driven parallel robots through cable angle sensors. In: Gosselin, C., Cardou, P., Bruckmann, T., Pott, A. (eds.) Cable-Driven Parallel Robots. Mechanisms and Machine Science, vol 53, pp. 167179. Springer (2018) DOI: 10.1007/978-3-319-61431-1_15
5. Sorenson, H. W.: Least-squares estimation: from Gauss to Kalman. IEEE Spectrum, 7(7), 63-68, (1970) DOI: 10.1109/MSPEC.1970.5213471
6. Merlet, J.P.: Some properties of the Irvine cable model and their use for the kinematic analysis of cable-driven parallel robots. Mechanism and Machine Theory, 135, 271280, (2019) DOI: 10.1016/j.mechmachtheory.2019.02.009

7. Pott, A.: Influence of pulley kinematics on cable-driven parallel robots. In: Lenarcic, J., Husty, M. (eds.) Latest Advances in Robot Kinematics, pp. 197204. Springer (2012) DOI: 10.1007/978-94-007-4620-6_25
8. Klimchik, A., Wu, Y., Abba, G., Garnier, S., Furet, B., Pashkevich, A.: Robust algorithm for calibration of robotic manipulator model, 7th IFAC Conference on Manufacturing Modelling, Management, and Control, pp. 808812. 19-21 June, Saint Petersburg, Russia (2013) DOI: 10.3182/20130619-3-RU-3018.00449
9. Idà, E., Carricato, M.: A New Performance Index for Underactuated Cable-Driven Parallel Robots. In: Gouttefarde, M., Bruckmann, T. (eds.) Cable-Driven Parallel Robots. CableCon 2021. Mechanisms and Machine Science, vol 104, pp. 24–36. Springer (2021) DOI: 10.1007/978-3-030-75789-2_3
10. Gabaldo, S., Idà, E., Carricato, M., Pose-estimation methods for underactuated cable-driven parallel robots, Mechanism and Machine Theory, 199, pp. 1-13 (2024) DOI: 10.1016/j.mechmachtheory.2024.105690
11. Verhoeven, R., Hiller, M., Tadokoro, S.: Workspace, stiffness, singularities and classification of tendon-driven stewart platforms. In: J. Lenari, M.L.H. (ed.) Advances in robot kinematics: Analysis and Control, pp. 105114. Springer (1998) DOI: 10.1007/978-94-015-9064-8_11
12. Silverman, B. W.: Density estimation for statistics and data analysis. Routledge (1998) DOI: 10.1201/9781315140919
13. Idà, E., Bruckmann, T., Carricato, M.: Rest-to-rest trajectory planning for underactuated cable-driven parallel robots. IEEE Transactions on Robotics 35(6), 13381351 (2019) DOI: 10.1109/TRO.2019.2931483